SCIENCE CHINA
Technological Sciences

•Article•

September 2019 Vol.62 No.9: 1483–1491
https://doi.org/10.1007/s11431-018-9468-8

# Energy harvesting via nonlinear energy sink for whole-spacecraft

ZHANG YeWei[1], LU YanNan[1] & CHEN LiQun[2*]

[1] *Faculty of Aerospace Engineerings, Shenyang Aerospace University, Shenyang 110136, China;*
[2] *School of Science, Harbin Institute of Technology, Shenzhen 518055, China*

Received September 1, 2018; accepted February 22, 2019; published online July 12, 2019

This paper presents nonlinear energy sink with giant magnetostrictive-piezoelectric material for energy harvesting of the whole-spacecraft vibration reduction system. The whole-spacecraft vibration attenuation system can effectively reduce vibration and achieve self-tuning enhanced energy harvesting range. The open-circuit voltage generated at low frequency is affected by the magnetic field force, alternating magnetic field and relative displacement. In order to acquire a steady periodic solution of the energy harvesting system, a combination of the harmonic balance method and pseudo arc length continuation technique is used. The numerical outcomes are consistent with the analytical outcomes in a certain range, which also proves the accuracy and reliability of the results. The amplitude and voltage of the energy harvesting system are analyzed by parameters such as cubic stiffness, viscous damping, and external excitation acceleration. In addition, this paper provides a new idea for broadband energy harvesting.

**nonlinear energy sink, giant magnetostrictive-piezoelectric material, pseudo arc length continuation technique, energy harvesting**

**Citation:** Zhang Y W, Lu Y N, Chen L Q. Energy harvesting via nonlinear energy sink for whole-spacecraft. Sci China Tech Sci, 2019, 62: 1483–1491, https://doi.org/10.1007/s11431-018-9468-8

## 1 Introduction

During the launch phase of a spacecraft, the spacecraft is subject to a variety of complex dynamic environmental loads. In order to reduce the environmental loads on the spacecraft launch, reduce the quality control cost of spacecraft and their equipment, and improve the reliability of spacecraft launch, vibration reduction and energy harvesting are of great significance to the whole spacecraft system.

As one of the green and renewable energy sources in the environment, vibration energy harvesting has received wide attention owing to its potential application prospects. Many types of energy convert to other forms of energy into electric energy, including thermomagnetoelectric [1], electromagnetic [2], piezoelectric electromagnetic [3]. There are other types of energy harvesting system [4–6].

Most previous studies have focused on linear vibration energy scavenging. Gatti et al. [7] considered linear energy harvesting attached a single-degree-of-freedom oscillator. Their results showed that maximum energy could be acquired near 17 Hz. Zhao et al. [8] made a series of optimization measures for linear energy harvesting systems and improved their performance. Chtiba et al. [9] investigated the integration of piezoelectric devices and linear structures and converted mechanical energy into electrical energy. Their work demonstrated that the vibration energy of the structure was limited to the vibration absorber and was acquired as electrical energy. The main drawback of linear energy scavenging was that the external excitation frequency was near to the resonance frequency, the maximum value of voltage and power could be generated.

Many researchers have applied nonlinear to energy harvesting system to realize broadband energy scavenging. The voltage and working frequency width of vibration energy

*Corresponding author (email: chenliqun@hit.edu.cn)

 

harvesting were improved through nonlinear vibration. Many advanced results have been shown. Qiu et al. [10] revealed that giant magnetoelectric hybrid vibration energy harvesting can effectively output the voltage and adjust the resonance frequency to realize broadband energy harvesting. Chu et al. [11] investigated giant magnetoelectric materials square-framed with four piezoelectric layers. Their work showed that this structure had multiple magnetoelectric resonant peaks and a broadband response in the range of 43–74 Hz. Li et al. [12] showed the broad bandhigh-sensitivity magnetostrictive/piezoelectric (PZT)/magnetoelectricive approach. It turns out that the broad range of resonant frequencies raised the control voltage region, and broadband energy harvesting was achieved.

Patil et al. [13] designed a broadband laminate structure with giant magnetoelectric materials and realized peaks of multiple resonance. The results demonstrated that anisotropic piezoelectric materials had a great influence on the response of resonant giant magnetostrictive materials with broadband. The shape and size of the giant magnetostrictive material had an influence on the resonance frequency [14]. Tao et al. [15] and Hu et al. [16] developed a 2DOF e-VEH MEMS device. This provided a new direction for the realization of MEMS broadband energy harvesting.

Magnetoelectric laminates which are a composite material composed of giant magnetostrictive-piezoelectric (GMMPZT) layers played a key role in broadband energy harvesting. The magnetostrictive layer and the piezoelectric layer had different layup directions along the thickness direction. Dong et al. [17] established a GMMPZT energy harvester, and the GMMPZT was transversely poled/magnetized (T-T mode). Magnetoelectric laminates were made of other models that were longitudinally magnetized, longitudinally poled (L-L mode) and transversely magnetized/longitudinally polarized (T-L mode) [18,19]. The magnetoelectric laminate's coefficient of the voltage in T-T mode was relatively lower than that of the T-L or L-L mode. The common characteristic is that the output energy is not high. In order to increase the output voltage of magnetoelectric laminates, an L-T model was established. The L-T model presented a higher output voltage and a more efficient harvesting of energy [20–23].

For the existing work, it is limited to energy harvesting of the single-degree-of-freedom with NES and the giant magnetostrictive material [24,25]. To test the broadband characteristics of nonlinear energy sink (NES), the whole-spacecraft needs to be equivalent to a two-degree-of-freedom model [26]. So it is necessary to vibration isolation and vibration reduction of the whole-spacecraft model. A nonlinear energy sink is a nonlinear vibration absorber with pure nonlinear stiffness [27], which has the advantage of wide frequency vibration absorption. In the NES system, a certain amount of energy is irreversibly transferred from an energy source to a receptor by means of targeted energy transfer. Integration of the targeted energy transfer and energy harvesting were explored to effectively acquire energy and isolate vibration. Ahmadabadi and Khadem [28] developed a beam structure comprising an NES and piezoelectric elements, and optimized the structural parameters. The NES and the giant magnetostrictive material were first associated, and the vibration energy was converted into magnetic energy and electrical energy. However, only the energy harvesting at the natural frequency is realized [24,25]. Li et al. [29] discussed the vibration attenuation and energy harvesting of an NES-piezoelectric system. Their work showed the possibility of vibration attenuation and vibration energy scavenging via integrating the NES and piezoelectric devices. Kremer and Liu [30,31] proved the performance of an energy harvesting system with an NES through numerical and experimental results. Their results realized vibration suppression and energy harvesting in broadband mode. Remick et al. [32] presented experimental and numerical studies of an electromechanical energy harvester with an NES. It turned out that reinforced vibration energy harvesting was acquired under an impulsive load. Xu et al. [33] proposed a hybrid energy harvesting system, which provided a new way for energy harvesting.

To analyze and predict the steady-state periodic solution of the system, the approximate analysis method needs to be used. At present, the analysis means mainly focus on the complexification-averaging method [25]. It is well-known that the method of harmonic balance has clear physical meaning. The present work will explore the application of the method of harmonic balance. However, the complicated nonlinear algebraic equations resulted from the harmonic balance analysis are hard to solve. The pseudo arc-length continuation is a powerful technique to overcome the difficulty. Zang et al. [34,35] introduced a combination of pseudo arc-length continuation and harmonic balance to analyze the dynamic characteristics of a single-degree-of-freedom (1DOF) system with an NES. Ding et al. [36,37] debated the steady-state response of a viscoelastic beam via the harmonic balance method with the pseudo arc-length continuation technique, and their results provided a promising direction for the vibration isolation of elastic systems.

This paper is based on the two-degree-of-freedom (2DOF) equivalent structure of the whole spacecraft structure. Compared with the 1DOF system, the 2DOF achieves broadband energy harvesting.

The other parts are arranged as follows. A dynamic analysis of the energy scavenging system is conducted in Section 2. The amplitude-frequency response curves with or without GMMPZT are compared and the open-circuit voltage at low frequency is analyzed in Section 3. The combination of the pseudo arc-length continuation and harmonic balance is introduced, and the effects of different parameters

on the amplitude-frequency response and open-circuit voltage are discussed in Section 4. The conclusion of this paper is presented in Section 5.

## 2 Dynamic analysis of energy harvesting system

The whole-spacecraft system is simplified to two substructures. One substructure is a spacecraft structure system, the other is a vibration isolator system. The 2DOF equivalent system of the whole-spacecraft structure with GMMPZT is showed in Figure 1(a). The whole-spacecraft system with the cubic stiffness is a nonlinear system. The L-T mode laminates of the structure are shown in Figure 1(b). The PZT layer is placed in the middle of two Terfenol-D layers. The thicknesses of the magnetostrictive and piezoelectric layers are $t_m$ and $t_p$. The magnetostrictive layers are magnetized in the length direction, and the piezoelectric layer is polarized in the lateral direction.

The energy harvesting system equation is

$$\begin{aligned} &m_1\ddot{x}_1 + c_1(\dot{x}_1 - \dot{x}_2) + k(x_1 - x_2) + m_1\ddot{x}_b = 0,\\ &m_2\ddot{x}_2 + c_1(\dot{x}_2 - \dot{x}_1) + c_2\dot{x}_2 + c_3(\dot{x}_2 - \dot{x}_3)\\ &+k_1(x_2 - x_1) + k_2x_2 + k_3(x_2 - x_3)^3 + F_m + m_2\ddot{x}_b = 0,\\ &m_3\ddot{x}_3 + c_3(\dot{x}_3 - \dot{x}_2) + k_3(x_3 - x_2)^3 - F_m + m_3\ddot{x}_b = 0, \end{aligned} \tag{1}$$

where $m_1$, $m_2$ and $m_3$ indicate the mass of the primary system, subsystem, and NES, respectively. $c_1$, $c_2$ and $c_3$ represent the viscous damping. $k_1$, and $k_2$ represent the linear stiffness and $k_3$ is the cubic stiffness. $F_m$ represents the nonlinear magnetic force. $x_b$ represents the excitation acceleration.

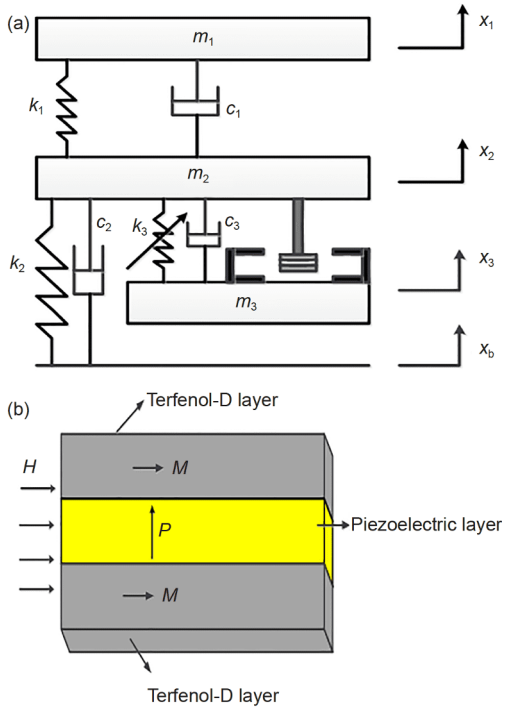


**Figure 1** (Color online) 2DOF equivalent system of (a) vibration energy harvesting and (b) magnetoelectric laminates.

$$\begin{aligned} x_b &= \frac{A}{(2\pi f)^2}\sin(2\pi ft),\\ \dot{x}_b &= \frac{A}{2\pi f}\cos(2\pi ft),\\ \ddot{x}_b &= -A\sin(2\pi ft). \end{aligned} \tag{2}$$

Firstly, the displacement magnetic force curve is obtained through numerical calculation, and then the expression of the magnetic force $F_m$ is obtained through curve fitting $F_m$. $F_m$ can be expressed by using a polynomial function [19]:

$$F_m = \sum_{j=0}^{5} a_j(x_2 - x_3)^j. \tag{3}$$

The displacement-magnetic induction intensity curve is obtained by a numerical method, and then the expression of magnetic induction intensity $B$ is obtained by fitting the curve [19].

$$B = \sum_{j=0}^{3} b_j(x_2 - x_3)^j, \tag{4}$$

where $b_0$=0.1959 T, $b_1$=37.63 T/m, $b_2$=−495.4 T/m$^2$ and $b_3$=−1.0151×10$^6$ T/m$^3$. $B(t)$ is comprised of the static and alternating magnetic sections. The static magnetic section provides a bias magnetic field for the laminate composite, and the alternating magnetic section generates the output voltage.

$$B(t) = B_s(t) + B_a(t), \tag{5}$$

where $B_s$ represents the static, and $B_a$ represents alternating magnetic sections, respectively. The open-circuit voltage $V_o(t)$ can be showed:

$$V_o(t) = \frac{\lambda\alpha_V}{\mu_0}B_a(t), \tag{6}$$

where $\alpha_V$ is the magnetoelectric coefficient. The theoretical magnetoelectric voltage coefficient is revised by the adjustment factors $\lambda$, $u_0$. $\alpha_V$ is expressed as follows:

$$\alpha_V = \frac{n(1-n)t_c d_{33,m}d_{31,p}}{\varepsilon_{33}\left[n\left(1-k_{31}^2\right)s_{11}^E + (1-n)s_{33}^H\right]}, \tag{7}$$

where $n = \frac{2t_m}{t_c}$ and $t_c = 2t_m + t_p$, $t_m$ and $t_p$ are the thicknesses of the piezoelectric and magnetostrictive layers, respectively; $t_c$ is the total thickness of the laminate; $s_{33}^E$ and $d_{33,m}$ are the longitudinal piezomagnetic elastic compliance and the piezomagnetic constant, respectively; and $s_{11}^E$, $d_{31,p}$, $\varepsilon_{33}$, $k_{31}$ are the piezoelectric elastic compliance, piezoelectric coefficient, permittivity tensor, and piezoelectric electromechanical coupling coefficient, respectively.

## 3 Comparative analysis and open-circuit voltage of 2DOF equivalent system of the whole-spacecraft structure

The NES with GMMPZT has an impact on vibration reduction in the whole-spacecraft structure from Figure 2. We found the following problems from Figures 2 and 3: (1) There is no peak at the low frequency of the amplitude-frequency response curve, but there is a peak at the low frequency of the voltage picture. (2) The amplitude-frequency response picture and the open-circuit voltage picture are normal near the natural frequency of 20 Hz. (3) The second-order natural frequency around 90 Hz is almost erased, but the voltage picture has a small peak near 90 Hz. In the amplitude-frequency response picture. This suggests that the energy is transferred to the nonlinear energy sink and the realization of broadband energy scavenging.

The system parameter are $m_1$=60 kg, $m_2$=12 kg, $k_1$=1.8677×10$^6$ N/m$^3$, $k_2$=2.1346×10$^6$ N/m, $c_1$=600 N s/m, $c_1$=20 N s/m, $m_3$=7 kg, $c_3$=600 N s/m, $k_3$=7×10$^9$ N/m$^3$ [24, 25].

The open-circuit voltage is showed in Figure 3. In order to figure out the open-circuit voltage at low frequency, the magnetic field force, alternating magnetic field, and relative displacements of $m_2$ and $m_3$ are compared at 1, 15 and 20 Hz. The results of Figures 4–6 present the same trend in the open-circuit voltage picture: 20 Hz>1 Hz>15 Hz. From the above results, the nonlinear energy sink with GMMPZT realize the integration of vibration control and energy harvesting. The magnetic field causes the relative displacement vibration amplitude of $m_2$ and $m_3$ to be larger at low frequency, and the corresponding voltage is larger. However, the amplitude-frequency response curve is not changed at low frequency, indicating that the energy is a targeted transfer from the main structure to the NES. Floating range of magnetic force in Figure 4. The alternating magnetic field range in Figure 5. The relative displacement picture of $m_2$ and $m_3$ in Figure 6:

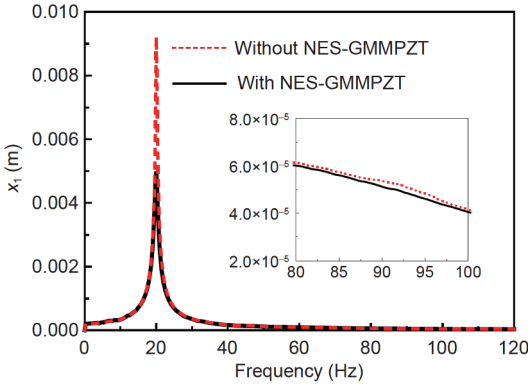


**Figure 2** Comparison of displacement in energy harvesting system with and without NES-GMMPZT.

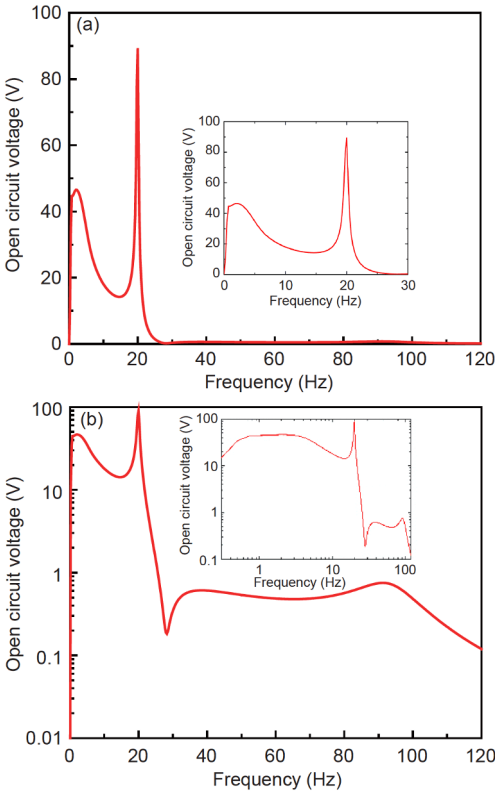


**Figure 3** Maximum voltage of open-circuit voltage (a) and enlargements (b).

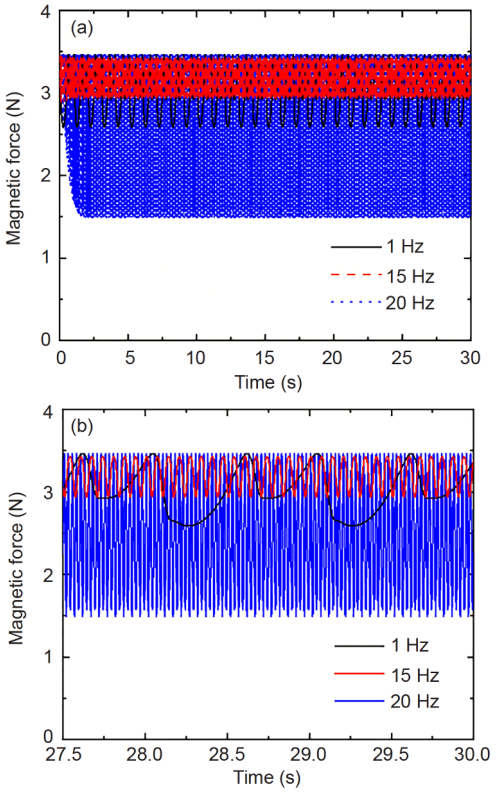


**Figure 4** Floating range of magnetic force (a) and enlargements (b): 20 Hz>1 Hz>15 Hz.

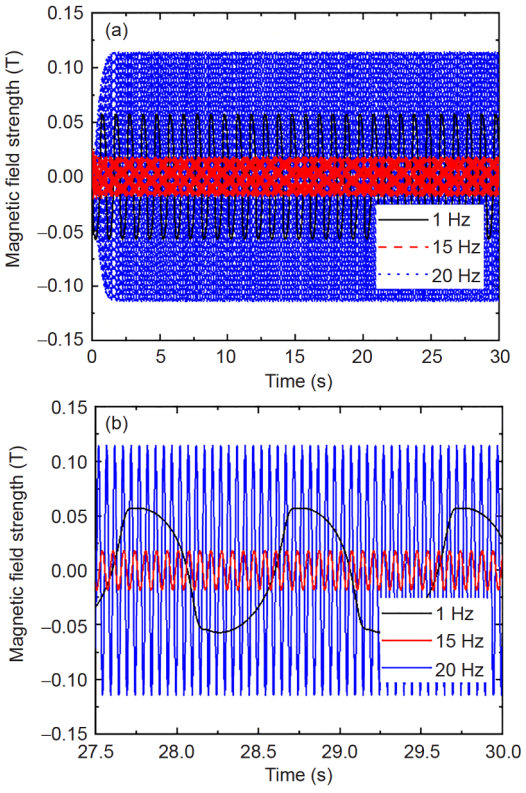


**Figure 5** Alternating magnetic field (a) and enlargements (b): 20 Hz> 1 Hz>15 Hz.

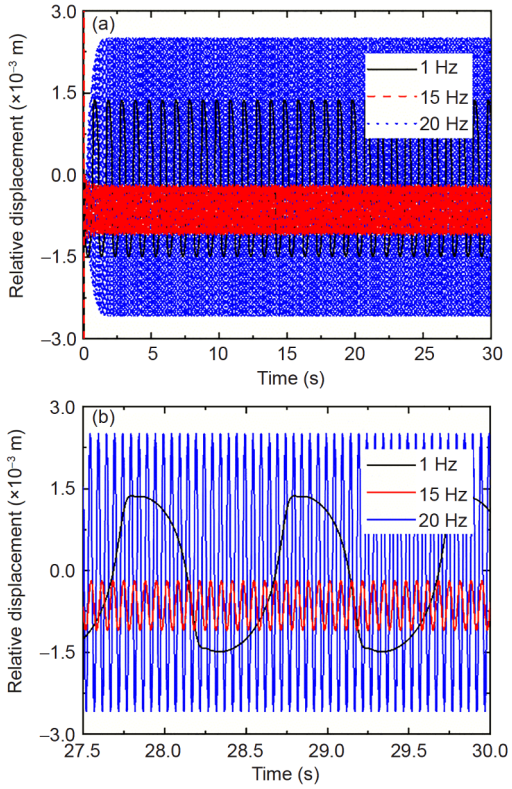


**Figure 6** Relative displacement amplitude range (a) and enlargements (b): 20 Hz>1 Hz>15 Hz.

## 4 Energy harvesting analysis of the whole-spacecraft structure by analytical technique

The dynamic responses of the main system equation need to be solved by using many low-harmonic terms. In order to study the convergence of simple harmonic polynomials, the solution of the differential equation is set to the third harmonic solution. Because the whole-spacecraft structure is nonlinear cubic, the approximate solution of the response only includes odd harmonic terms. In order for the numerical results to converge more quickly, the solution of the ordinary differential equation is chosen as the three cubic harmonic solutions. Preserving the third harmonic term is accurate enough based on refs. [32–34] as follows:

$$\begin{aligned} x_1(t) &= a_{11}\cos(\omega t) + b_{11}\sin(\omega t) + a_{31}\cos(3\omega t) \\ &\quad + b_{31}\sin(3\omega t), \\ x_2(t) &= a_{12}\cos(\omega t) + b_{12}\sin(\omega t) + a_{32}\cos(3\omega t) \\ &\quad + b_{32}\sin(3\omega t), \\ x_3(t) &= a_{13}\cos(\omega t) + b_{13}\sin(\omega t) + a_{33}\cos(3\omega t) \\ &\quad + b_{33}\sin(3\omega t), \end{aligned} \tag{8}$$

where $a_{ij}$ and $b_{ij}$ are constant terms of the corresponding harmonic polynomial. The harmonic polynomials eq. (8) is brought into eq. (1). The coefficients of $\cos(i\omega t)$ and $\sin(i\omega t)$ ($i$=1, 3) of the resulting equations are zero and are presented as eq. (8). The nonlinear algebraic equations need to be solved by using the pseudo arc-length continuation, but Newton iterative method cannot effectively pass the inflection point of amplitude-frequency response. Therefore, the whole amplitude response frequency band can be obtained by pseudo arc-length continuation technique. The pseudo arc-length continuation technique is introduced in order to acquire the harmonic coefficients in the harmonic solution of eq. (8). The pseudo arc-length continuation technique is used to solve eq. (8) according to the Newton iteration method. The coefficient of eq. (8) is too much and omitted. The pseudo arc-length continuation technique has a distinct advantage in solving multivalued issues because its iteration is directional. The amplitude expression of the primary system is showed:

$$\begin{aligned} x_{1A} &= \sqrt{a_{11}^2 + b_{11}^2 + a_{31}^2 + b_{31}^2}, \\ x_{2A} &= \sqrt{a_{12}^2 + b_{12}^2 + a_{32}^2 + b_{32}^2}, \\ x_{3A} &= \sqrt{a_{13}^2 + b_{13}^2 + a_{33}^2 + b_{33}^2}. \end{aligned} \tag{9}$$

A comparison is made of the numerical and analytical results to verify the correctness of the results. Figure 7 shows a comparison of the numerical outcome of the fourth-order Runge-Kutta algorithm and the analytical outcomes of the harmonic balance technique. The numerical outcomes are consistent with the analytical outcomes in a certain range in Figure 7. Under any circumstances, Figure 7 indicates that

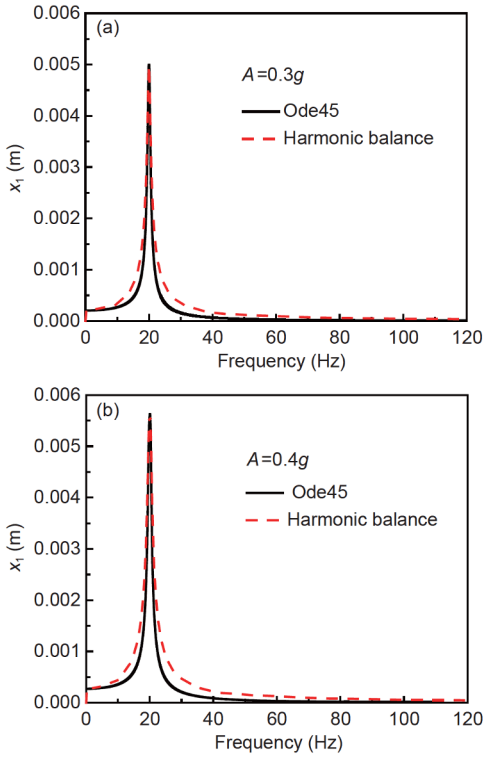


**Figure 7** (Color online) Comparison of numerical and analytical solutions under different acceleration excitation conditions.

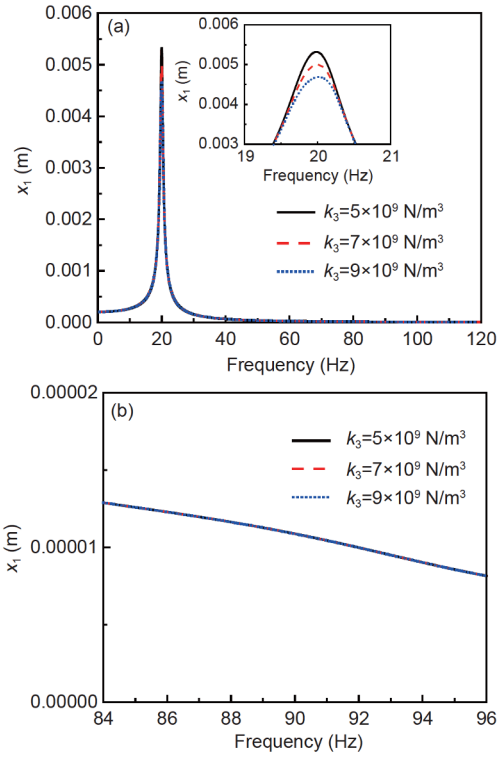


**Figure 8** (Color online) Amplitude-frequency response curves (a) and the enlargement (b) as the cubic stiffness changes.

both the approximate analytical outcome and the numerical outcome are correct and reliable.

### 4.1 Parameter analysis

The analysis of the parameters has a great effect on the dynamic behavior and energy harvesting. The change of parameter in the energy harvesting system is discussed as follows.

Figure 8 reveals the variation of the amplitude-frequency response picture in the different stiffness conditions. It can be seen from Figure 8 that the amplitude decreases with the nonlinear stiffness increasing. There is a negative correlation between the nonlinear stiffness and the amplitude. When the frequency is close to 90 Hz, the stiffness has little effect.

The change of voltage with the stiffness varying is shown in Figure 9. The nonlinear stiffness has little effect on the value of the voltage, but the nonlinear stiffness plays a key role in energy transfer.

The amplitude frequency response curves under different damping conditions are shown in Figure 10. With the increase of damping, the amplitude gradually decreases. The results indicate that the increase of damping always has a positive correlation.

Figure 11 indicates that the open-circuit voltage varies as the damping increases. As the damping increases, the voltage decreases. This is the opposite of the amplitude-frequency

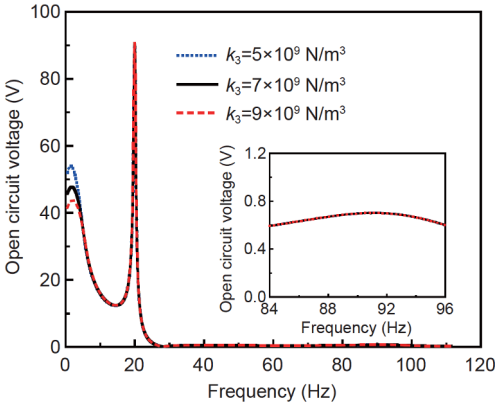


**Figure 9** (Color online) Open-circuit voltage curves as cubic stiffness changes and enlargement.

response. It is shown that more energy is transferred to the energy harvesting system as the damping decreases. These results are exactly opposite to those near 20 Hz at high frequency.

Figure 12 shows the amplitude-frequency response as the mass changes. As the mass increases, the amplitude decreases and presents a negative correlation. The change of mass at high frequency has no effect on the amplitude.

Figure 13 shows that the open-circuit voltage changes with mass increasing. With the mass decreasing, the open-circuit voltage gradually increases. Meanwhile, Figure 13 shows that the mass can reduce the resonance peak of the open-

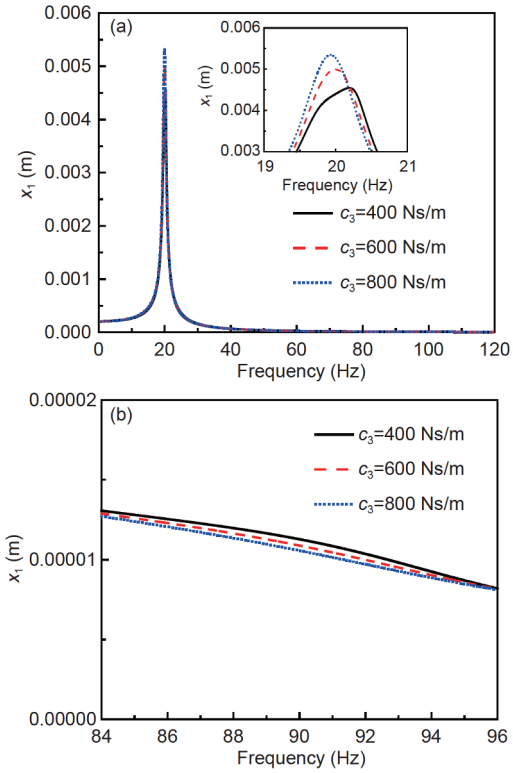


**Figure 10** (Color online) Amplitude-frequency response curves of (a) and enlargement (b) as the damping varies.

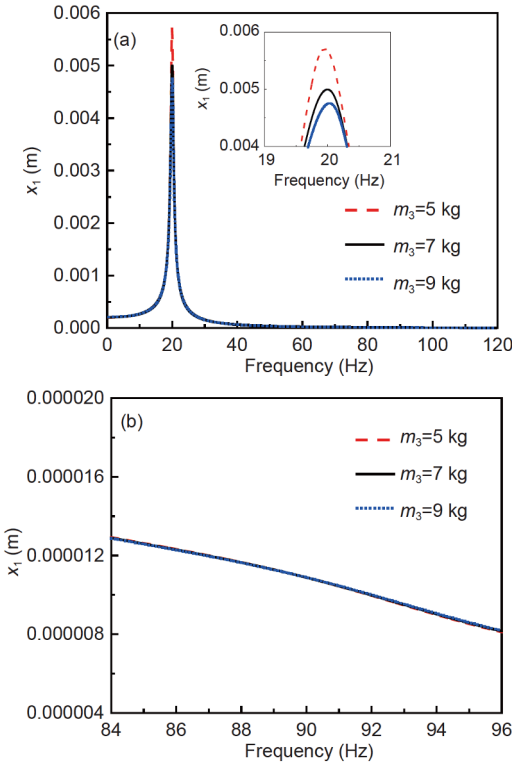


**Figure 12** (Color online) Amplitude-frequency response curves (a) and (b) as mass of NES changes.

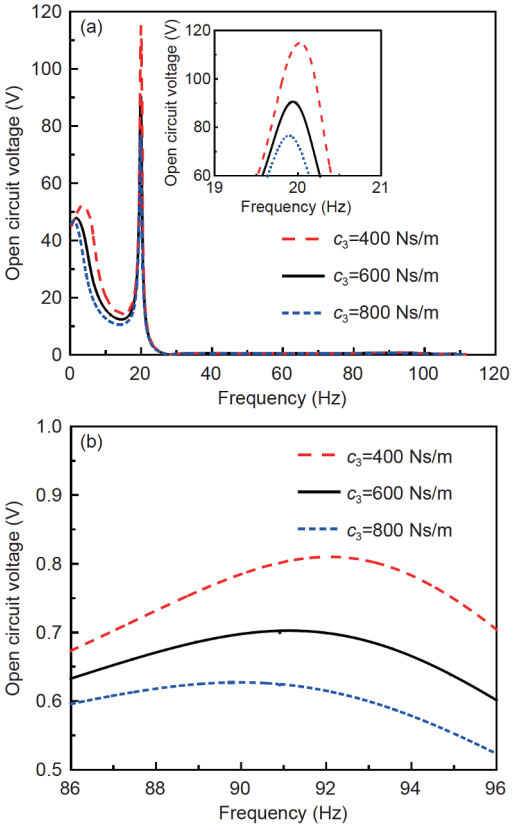


**Figure 11** (Color online) Open-circuit voltage curves of (a) and enlargements (b) when damping changes.

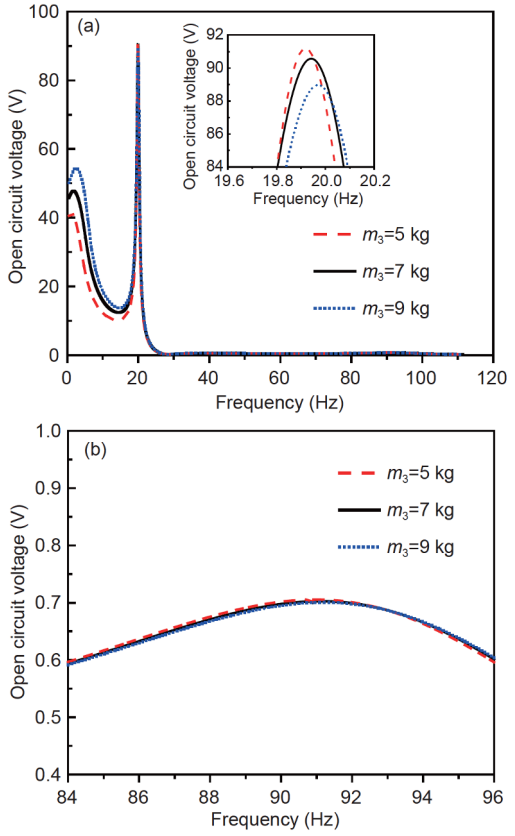


**Figure 13** (Color online) The open circuit voltage curves (a) and enlargement (b) as the mass changes.

circuit voltage. The mass has little impact on the open-circuit voltage at high frequency.

Figure 14 displays amplitude-frequency response change under different acceleration conditions. Figure 14 shows that the amplitude increases with excitation acceleration increasing.

Figure 15 shows the change of the open-circuit voltage with different acceleration changing. The open-circuit voltage augments with the raise of the excitation acceleration. The excitation acceleration has a great influence on the open-circuit voltage.

It can be seen from the result of parameter analysis. The displacement change at high frequency is very small, the mass and stiffness have little influence on the high frequency, but it is very important to the energy transfer of the system [23]. The change of damping plays an important role in distributing and regulating the displacement and voltage.

Amplitude-frequency response curve keeps straight without skewness because the nonlinearity is not very strong and such performance has been previously reported [27,38].

## 5 Conclusions

In this work, the integration of nonlinear energy sink and giant magnetostrictive-piezoelectric material is proposed for energy harvesting and vibration reduction of the whole-spacecraft vibration reduction system. The magnetic field force, alternating magnetic field, and relative displacement impact the open-circuit voltage. A combination of the harmonic balance method and pseudo arc-length continuation technique is introduced to acquire the stable periodic solution of the system. Different parameters have an effect on the voltage and amplitude of the energy harvesting system. The following conclusions can be drawn.

(1) The 2DOF equivalent system of the whole-spacecraft structure realizes broadband energy harvesting and achieves self-tuning enhanced energy harvesting range.

(2) The bias magnetic field of the giant magnetostrictive material has a great impact on the material. The higher voltage at low frequency is a result of the higher alternating magnetic field at this frequency.

(3) The harmonic balance and pseudo arc-length continuation techniques are first applied to a magnetoelectromechanical coupling system. There is a consistent trend between the numerical solutions and analytical solutions in a certain range.

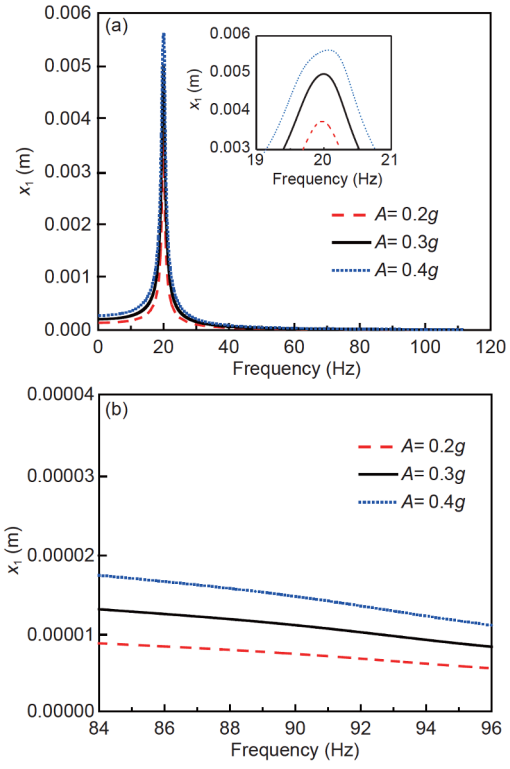


**Figure 14** (Color online) Amplitude-frequency response curves of (a) and enlargements (b) as acceleration changes.

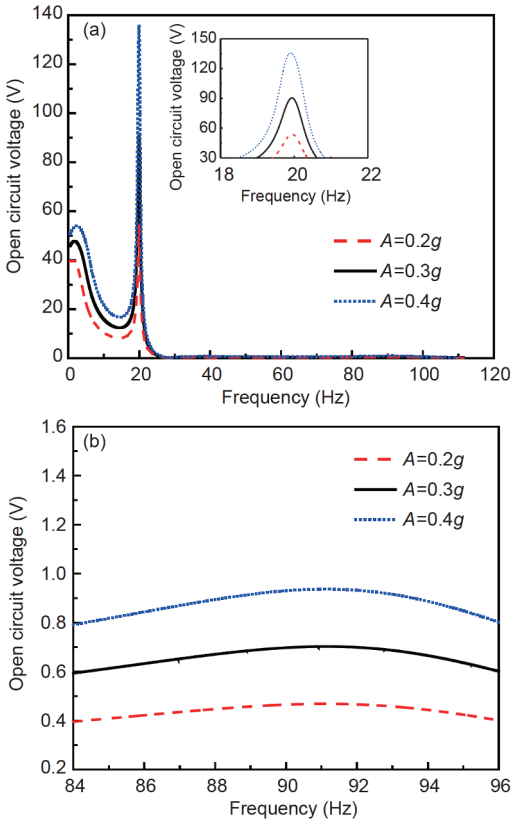


**Figure 15** (Color online) Open-circuit voltage curves of (a) and enlargements (b) when acceleration changes.

*This work was supported by the National Natural Science Foundation of China (Grant Nos. 11772205, 11572182, 51775541, 11672188), the Scientific Research Fund of Liaoning Provincial Education Department (Grant Nos. L201703, L201737, L201762), and the Liaoning Revitalization Talents Program (Grant No. XLYC1807172).*

1 Chun J, Song H C, Kang M G, et al. Thermo-Magneto-Electric generator arrays for active heat recovery system. Sci Rep, 2017, 7: 41383
2 Naifar S, Bradai S, Viehweger C, et al. Survey of electromagnetic and magnetoelectric vibration energy harvesters for low frequency excitation. Measurement, 2017, 106: 251–263
3 Li P, Gao S Q, Cai H T. Modeling and analysis of hybrid piezoelectric and electromagnetic energy harvesting from random vibrations. Microsyst Technol, 2015, 21: 401–414
4 Zhou S X, Zuo L. Nonlinear dynamic analysis of asymmetric tristable energy harvesters for enhanced energy harvesting. Commun Nonlinear Sci Numer Simul, 2018, 61: 271–284
5 Tran N, Ghayesh M H, Arjomandi M. Ambient vibration energy harvesters: A review on nonlinear techniques for performance enhancement. Int J Eng Sci, 2018, 127: 162–185
6 Pan P, Zhang D B, Nie X, et al. Development of piezoelectric energy-harvesting tuned mass damper. Sci China Tech Sci, 2017, 60: 467–478
7 Gatti G, Brennan M J, Tehrani M G, et al. Harvesting energy from the vibration of a passing train using a single-degree-of-freedom oscillator. Mech Syst Signal Process, 2016, 66-67: 785–792
8 Zhao L, Tang L, Yang Y. Comparison of modeling methods and parametric study for a piezoelectric wind energy harvester. Smart Mater Struct, 2013, 22: 125003
9 Chtiba M O, Choura S, Nayfeh A H, et al. Vibration confinement and energy harvesting in flexible structures using collocated absorbers and piezoelectric devices. J Sound Vib, 2010, 329: 261–276
10 Qiu J, Tang X, Chen H, et al. A tunable broadband magnetoelectric and electromagnetic hybrid vibration energy harvester based on nanocrystalline soft magnetic film. Surf Coatings Tech, 2016, 320: 447–451
11 Chu Z, Gao X, Shi W, et al. A square-framed ME composite with inherent multiple resonant peaks for broadband magnetoelectric response. Sci Bull, 2017, 62: 1177–1180
12 Li P, Wen Y, Huang X, et al. Wide-bandwidth high-sensitivity magnetoelectric effect of magnetostrictive/piezoelectric composites under adjustable bias voltage. Senss Actuators A-Phys, 2013, 201: 164–171
13 Patil D R, Kambale R C, Chai Y, et al. Multiple broadband magnetoelectric response in thickness-controlled Ni/[011] $Pb(Mg_{1/3}Nb_{2/3})O_3$-$Pb(Zr,Ti)O_3$ single crystal/Ni laminates. Appl Phys Lett, 2013, 103: 052907
14 Dong S, Zhai J, Li J F, et al. Small dc magnetic field response of magnetoelectric laminate composites. Appl Phys Lett, 2006, 88: 082907
15 Tao K, Tang L, Wu J, et al. Investigation of multimodal electret-based mems energy harvester with impact-induced nonlinearity. J Microelectromech Syst, 2018, 27: 276–288
16 Hu W, Zhang C, Wang Z L. Recent progress in piezotronics and tribotronics. Nanotechnology, 2018, 30: 042001
17 Dong S, Zhai J, Xing Z, et al. Magnetoelectric laminate composites-enhanced magnetic field sensitivity and high voltage gain. In: Symposium CC—Coupled Nonlinear Phenomena Modeling and Simulation for Smart, Ferroic and Multiferroic Materials. MRS Proceedings, Volume 881. Cambridge: Cambridge University Press, 2005. 1–14
18 Palneedi H, Annapureddy V, Priya S, et al. Status and perspectives of multiferroic magnetoelectric composite materials and applications. Actuators, 2016, 5: 9–31
19 Dong S, Li J F, Viehland D. Longitudinal and transverse magnetoelectric voltage coefficients of magnetostrictive/ piezoelectric laminate composite: Experiments. IEEE Trans Ultrason Ferroelectr Freq Control, 2004, 51: 794–799
20 Dai X, Wen Y, Li P, et al. Modeling, characterization and fabrication of vibration energy harvester using Terfenol-D/PZT/Terfenol-D composite transducer. Senss Actuators A-Phys, 2009, 156: 350–358
21 Chu Z, Shi H, Shi W, et al. Enhanced resonance magnetoelectric coupling in (1-1) connectivity composites. Adv Mater, 2017, 29: 1606022
22 Zhou H M, Li M H, Zhou Y, et al. Nonlinear resonant magnetoelectric coupling model for dual-peak phenomenon in magnetoelectric laminates. J Alloys Compd, 2016, 672: 292–297
23 Yang J, Wen Y M, Li P, et al. A magnetoelectric-based broadband vibration energy harvester for powering wireless sensors. Sci China Tech Sci, 2011, 54: 1419–1427
24 Fang Z W, Zhang Y W, Li X, et al. Integration of a nonlinear energy sink and a giant magnetostrictive energy harvester. J Sound Vib, 2017, 391: 35–49
25 Fang Z W, Zhang Y W, Li X, et al. Complexification-averaging analysis on a giant magnetostrictive harvester integrated with a nonlinear energy sink. J Vib Acoust, 2017, 140: 021009
26 Yang K, Zhang Y W, Ding H, et al. Nonlinear energy sink for whole-spacecraft vibration reduction. J Vib Acoust, 2017, 139: 021011
27 Chen J E, He W, Zhang W, et al. Vibration suppression and higher branch responses of beam with parallel nonlinear energy sinks. Nonlinear Dyn, 2018, 91: 885–904
28 Ahmadabadi Z N, Khadem S E. Nonlinear vibration control and energy harvesting of a beam using a nonlinear energy sink and a piezoelectric device. J Sound Vib, 2014, 333: 4444–4457
29 Li X, Zhang Y, Ding H, et al. Integration of a nonlinear energy sink and a piezoelectric energy harvester. Appl Math Mech-Engl Ed, 2017, 38: 1019–1030
30 Kremer D, Liu K. A nonlinear energy sink with an energy harvester: Transient responses. J Sound Vib, 2014, 333: 4859–4880
31 Kremer D, Liu K. A nonlinear energy sink with an energy harvester: Harmonically forced responses. J Sound Vib, 2017, 410: 287–302
32 Remick K, Quinn D D, McFarland D M, et al. High-frequency vibration energy harvesting from impulsive excitation utilizing intentional dynamic instability caused by strong nonlinearity. J Sound Vib, 2016, 370: 259–279
33 Xu X, Zhang C, Han Q, et al. Hybrid energy harvesting from mechanical vibrations and magnetic field. Appl Phys Lett, 2018, 113: 013901
34 Zang J, Chen L Q. Complex dynamics of a harmonically excited structure coupled with a nonlinear energy sink. Acta Mech Sin, 2017, 33: 801–822
35 Zang J, Zhang Y W, Ding H, et al. The evaluation of a nonlinear energy sink absorber based on the transmissibility. Mech Syst Signal Processing, 2019, 125: 99–122
36 Ding H, Zhu M H, Chen L Q. Nonlinear vibration isolation of a viscoelastic beam. Nonlinear Dyn, 2018, 92: 325–349
37 Ding H, Tang Y Q, Chen L Q. Frequencies of transverse vibration of an axially moving viscoelastic beam. J Vib Control, 2017, 23: 3504–3514
38 Parseh M, Dardel M, Ghasemi M H. Performance comparison of nonlinear energy sink and linear tuned mass damper in steady-state dynamics of a linear beam. Nonlinear Dyn, 2015, 81: 1981–2002